J. Fluid Mech. (2010), *vol.* 656, *pp.* 448–457.
doi:10.1017/S0022112010002703

Charney isotropy and equipartition in quasi-geostrophic turbulence

ANDREAS VALLGREN† AND ERIK LINDBORG

Linné FLOW Centre, KTH Mechanics, SE-100 44 Stockholm, Sweden

(Received 25 March 2010; revised 3 May 2010; accepted 5 May 2010;
first published online 1 July 2010)

High-resolution simulations of forced quasi-geostrophic (QG) turbulence reveal that Charney isotropy develops under a wide range of conditions, and constitutes a preferred state also in β-plane and freely decaying turbulence. There is a clear analogy between two-dimensional and QG turbulence, with a direct enstrophy cascade that is governed by the prediction of Kraichnan (*J. Fluid Mech.*, vol. 47, 1971, p. 525) and an inverse energy cascade following the classic $k^{-5/3}$ scaling. Furthermore, we find that Charney's prediction of equipartition between the potential and kinetic energy in each of the two horizontal velocity components is approximately fulfilled in the inertial ranges.

Key words: rotating turbulence, turbulence simulation, turbulence theory

1. Introduction

Quasi-geostrophic (QG) turbulence is fundamental for the understanding of atmospheric dynamics at planetary and synoptic scales. As demonstrated by Charney (1971), QG turbulence has a lot in common with two-dimensional turbulence, with a direct cascade of potential enstrophy and an inverse cascade of energy. Ever since Nastrom & Gage (1985) and Gage & Nastrom (1986) presented observations on the atmospheric kinetic energy spectrum, attempts have been made to explain the scaling of the energy spectrum in terms of QG turbulence (e.g. Tung & Orlando 2003), or two-dimensional turbulence (e.g. Lilly 1989; Lindborg 1999). Despite the difficulties in obtaining a convincing theory for the scaling of the atmospheric energy spectrum, QG turbulence theory is interesting in its own right. It has a richness beyond that of either three-dimensional isotropic turbulence or two-dimensional turbulence. This paper deals with the original formulation of QG scaling by Charney (1971) and intends to investigate, perhaps, the strongest predictions; that of 'Charney isotropy' and equipartition between the potential and kinetic energy in each of the two horizontal components. Charney isotropy refers to isotropic scaling of the potential and kinetic energy spectra, when the vertical coordinate has been scaled by a factor N/f, where N is the basic state Brunt–Väisälä frequency and f is the Coriolis parameter. Charney's prediction of isotropy in the enstrophy inertial range was supported by Hua & Haidvogel (1986), who simulated QG flow on a β-plane. This result was later confirmed by studies such as McWilliams (1989), who also demonstrated the similarities with two-dimensional turbulence regarding cascade directions. The QG flows are rich in structures such as vortices, and the statistics of

† Email address for correspondence: vallgren@mech.kth.se

these have been explored by, for example, McWilliams (1990), McWilliams, Weiss & Yavneh (1999), Dritschel, de la Torre Juarez & Ambaum (1999), von Hardenberg *et al.* (2000) and Reinaud, Dritschel & Koudella (2003). We will complement these studies by testing the prediction of Charney isotropy and equipartition. To do this, we will perform a set of very high resolution direct numerical simulations of the QG potential vorticity equation, under a wide range of conditions.

2. Numerical method

We simulate the Charney QG potential vorticity equation, with the inclusion of a random and white in time forcing. Ultraviolet dissipation of potential enstrophy is accomplished by the use of hyperviscosity. Infrared dissipation of energy is maintained by an optional linear Ekman drag. To allow for the study of β-plane dynamics, we have included the β-term as an optional term in our simulations. Thus, the simulated equation is

$$\frac{\partial q}{\partial t} + (\boldsymbol{u_h} \cdot \nabla_h)\, q + \beta v = -\nu \Delta^2 q + f - \alpha q, \tag{2.1}$$

where

$$q = \nabla^2 \psi \tag{2.2}$$

is the QG potential vorticity, Δ is the three-dimensional Laplace operator in scaled coordinates, ψ is the stream function, $\boldsymbol{u_h} = u\boldsymbol{e_x} + v\boldsymbol{e_y} = -\partial_y \psi \boldsymbol{e_x} + \partial_x \psi \boldsymbol{e_y}$ is the horizontal velocity and ∇_h the horizontal gradient operator, ν is the hyperviscosity coefficient and α is an Ekman drag coefficent. The simulations are performed using a pseudospectral code with triply periodic boundary conditions, 8/9 dealiasing in the horizontal directions (see e.g. McWilliams 1989) and fourth-order Runge–Kutta time stepping. The potential enstrophy injection rate, η, is controlled at each time step by requiring that $\langle q f_q \rangle = 0$, where $\langle . \rangle$ is the average over the box (see Alvelius 1999 for more details regarding the forcing algorithm). The enstrophy injection rate is set to $\eta = 1$, and time is non-dimensionalized by $\eta^{-1/3} = 1$. The forcing is localized in a spherical shell in Fourier space, so that both barotropic and baroclinic modes are forced. The forcing is thus Charney isotropic and injects twice as much kinetic as potential energy into the system. The simulations are all performed with a resolution of 1024^3 grid points. Our main simulations are presented in table 1, and they will be referred to as $X1024YZ$, where $X = S$ or L depending on whether small-scale (S) or large-scale (L) forcing is used, $Y = E$ if Ekman drag is active and $Z = B$ if $\beta > 0$, otherwise no indices Y, Z are used.

3. Results

We begin by presenting the results from two simulations where we force at small wavenumbers $k \in [5, 9]$, centred at $k_f = 7$, endeavoured to study the enstrophy cascade regime in QG turbulence. One of the simulations, $L1024E$, has an isotropic large-scale drag imposed, and one is without such a drag ($L1024$). In both cases, we obtain quasi-stationary enstrophy cascade ranges after about 60 non-dimensional time units, as can be seen in figure 1. However, while energy is growing linearly in $L1024$, it reaches a quasi-stationary state in $L1024E$ after approximately 250 non-dimensional time units. Potential energy reaches stationarity much earlier in both simulations. The potential enstrophy fluxes are presented in figure 2. They are almost constant over a little bit more than one decade, and in this range – the enstrophy cascade range – both

Run	k_f	ν	α	t_{max}	$\mathscr{K}$	$\mathscr{K}'$	k_L	ϵ_q^L	ϵ_q	Ω	E_k	E_p
$L1024$	7	4.0×10^{-19}	0	120	–	2.89	4.5	0	1.00	13.2	Incr.	0.12
$L1024E$	7	1.0×10^{-19}	8.0×10^{-3}	316	–	2.88	5.6	0.20	0.80	12.5	1.22	0.10
$L1024EB$	7	2.0×10^{-20}	8.0×10^{-3}	170	–	3.33	7.9	0.26	0.74	15.8	1.10	0.20
$S1024$	107	4.0×10^{-19}	0	1223	7.0	–	–	0	1.00	6.8	Incr.	0.005
$S1024E$	107	4.0×10^{-19}	1.3×10^{-3}	1304	7.0	–	–	0.02	0.98	8.1	0.023	0.004
$S1024EB$	107	2.0×10^{-20}	1.3×10^{-3}	1000	5.2	–	–	0.02	0.98	9.0	0.023	0.004
$L1024EF$	(7)	1.0×10^{-19}	0	227	–	2.75	8.6	Decr.	Decr.	Decr.	1.3	0.021
$L1024F$	(13)	2.0×10^{-21}	0	366	–	3.26	12.1	Decr.	Decr.	Decr.	0.004	0.002

TABLE 1. Stationary statistics from the simulations. The wavenumber k_f represents the main forcing wavenumber (parentheses indicate initial peak distribution for decaying cases), t_{max} is how long time a simulation has been run, ϵ_q^L is the potential enstrophy dissipation due to the Ekman drag, Ω is the mean potential enstrophy, E_k is the mean kinetic energy and E_p is the mean potential energy. Decr., decreasing; Incr., increasing. The remaining parameters are introduced in the text.

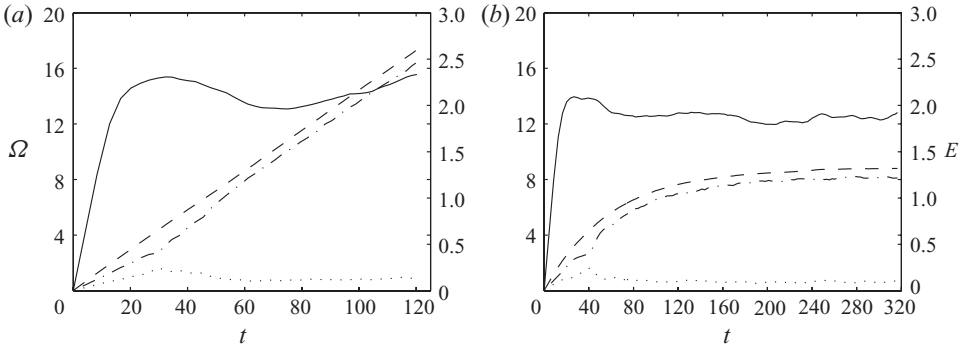

FIGURE 1. Temporal evolution of potential enstrophy (solid line), total energy (dashed), kinetic (dash-dotted) and potential (dotted) energy for $L1024$ (a) and $L1024E$ (b).

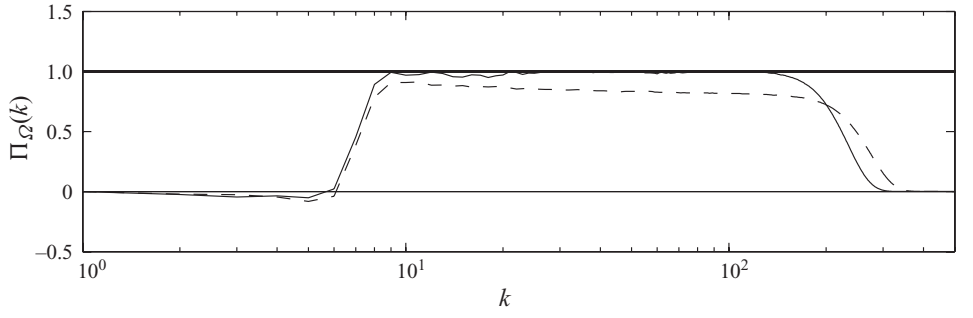

FIGURE 2. Potential enstrophy flux for the two simulations $L1024$ (solid) and $L1024E$ (dashed). Zero and unity lines are indicated.

simulations show a logarithmically corrected Charney isotropic k^{-3} energy spectrum for both kinetic and potential energy (see figure 3; only total energy shown). The k^{-3} scaling with a logarithmic correction (as anticipated by Herring 1980) is much like

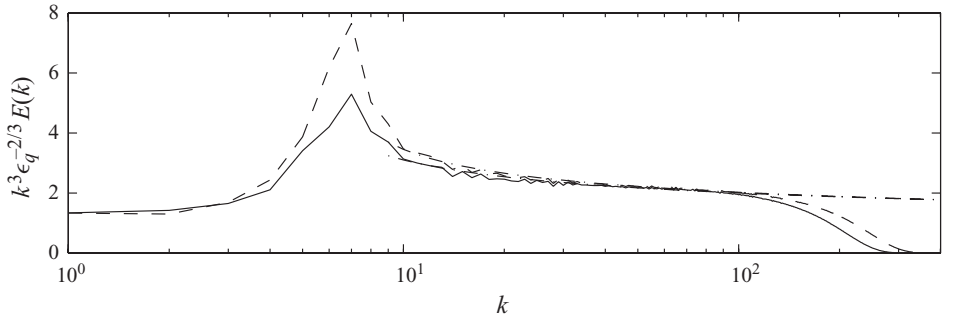

FIGURE 3. Compensated energy spectra, $k^3\epsilon_q^{-2/3}E(k)$, for $L1024$ (solid) and $L1024E$ (dashed) together with Kraichnan logarithmic fits (dash-dotted).

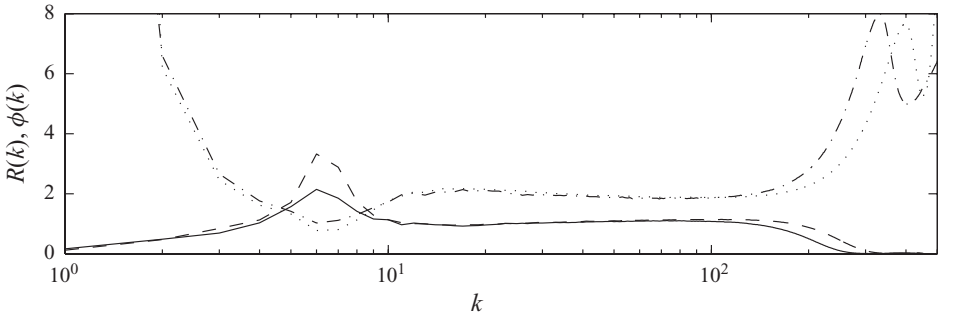

FIGURE 4. $R(k)$ for $L1024$ (solid), $L1024E$ (dashed) and $\phi(k)$ for $L1024$ (dash-dotted) and $L1024E$ (dotted).

that expected in two-dimensional turbulence (Kraichnan 1971), i.e.

$$E(k) = \mathscr{K}'\epsilon_q^{2/3}k^{-3}[\ln(k/k_L)]^{-1/3}\,, \tag{3.1}$$

where the Kraichnan coefficient $\mathscr{K}'$ is estimated to 2.9, ϵ_q is the potential enstrophy dissipation rate and k_L is approximately equal to the lowest forcing wavenumber. Figure 4 shows the ratio

$$R(k) = \frac{E_z(k)}{E_h(k)}, \tag{3.2}$$

where $E_z(k)$ is the one-dimensional vertical energy spectrum and $E_h(k)$ is the one-dimensional horizontal energy spectrum. Figure 4 also shows the ratio

$$\phi(k) = \frac{E_k(k)}{E_p(k)}, \tag{3.3}$$

where $E_k(k)$ and $E_p(k)$ are the three-dimensional kinetic and potential energy spectra, respectively. In the enstrophy cascade range, $R(k)$ is close to unity, which is consistent with Charney isotropy. At the forcing wavenumber, however, and at smaller wavenumbers, Charney isotropy is not valid, although the forcing itself is Charney isotropic. The ratio $\phi(k)$ is close to two in the inertial range, which is consistent with equipartition. At the forcing scales, however, $\phi(k)$ is approximately equal to unity, although the forcing injects twice as much kinetic as potential energy. As for the energy fluxes, an inverse energy cascade towards smaller wavenumbers is observed in the very limited range $k < 5$, for both the potential and kinetic energy

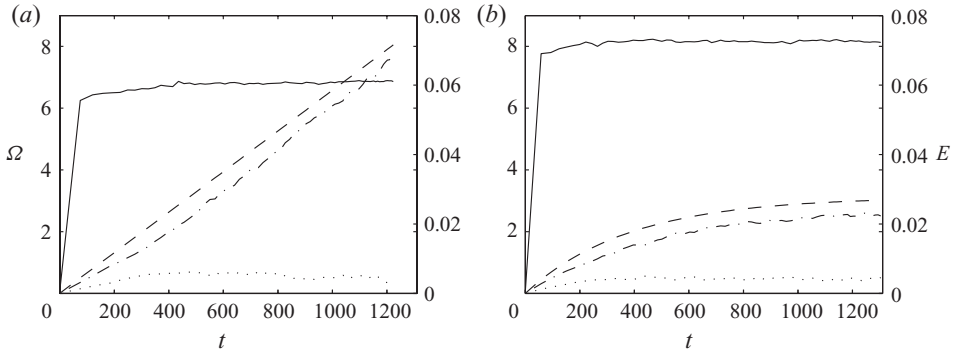

FIGURE 5. Temporal evolution of potential enstrophy (solid), total energy (dashed), kinetic (dash-dotted) and potential energy (dotted) for $S1024$ (a) and $S1024E$ (b).

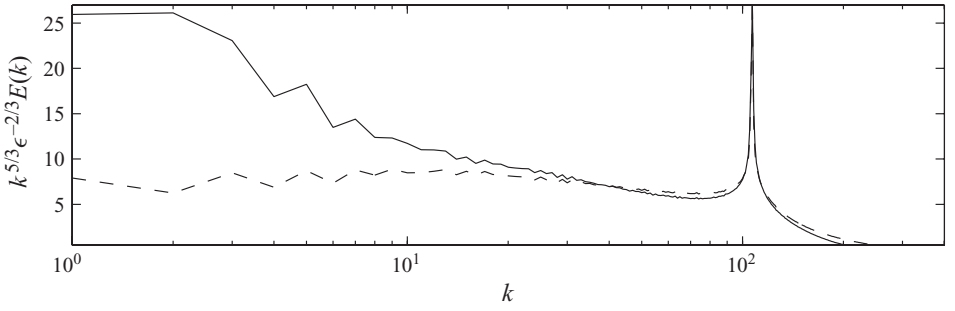

FIGURE 6. Compensated energy spectra, $k^{5/3}\epsilon^{-2/3}E(k)$, for $S1024$ (solid) and $S1024E$ (dashed).

(not shown). However, there is a continuous transfer of potential energy to kinetic energy, corresponding to a barotropization of the flow at large scales (as also found by Smith & Waleffe 1999). The effects of this transfer become clear by investigating the potential vorticity distribution in real space (see figure 9a). We see the presence of two dominating structures with opposite sign, which tend to organize in the vertical. The presence of a drag in the $L1024E$-simulation slightly suppresses the growth of these structures. We also see the filamentary debris surrounding these. The fine-scale structure of the flow is illustrated in figure 10, showing the horizontal and vertical cross-sections of potential vorticity, revealing the richness of the flow.

In our second set of simulations, $S1024$ and $S1024E$, the inverse energy cascade is investigated. Here, the forcing is in a narrow range $k \in [105, 109]$, centred at $k_f = 107$. Once again, we perform one simulation with Ekman drag ($S1024E$) and one without ($S1024$). Potential enstrophy quickly reaches quasi-stationarity (see figure 5), as the forcing is much closer to the dissipation range, whereas the energy reaches stationarity much later, after about 300 non-dimensional time units for the potential energy (both simulations) and approximately 1000 time units for the kinetic energy in case of an Ekman drag ($S1024E$). The corresponding energy flux (figure 7, showing $S1024E$; $S1024$ is qualitatively identical) is mostly towards larger scales with essentially one and a half decade of stationary energy flux. There is also a small but not insignificant portion that escapes towards smaller scales. The energy spectra quickly evolves into nearly Charney isotropic states, with $R(k) \sim 2/3$ (see figure 8) and roughly $\sim k^{-5/3}$ scaling, with a tendency towards a little steeper spectrum for the kinetic energy part (not shown, but reflected in figure 6). In particular, this is the case in $S1024$, where

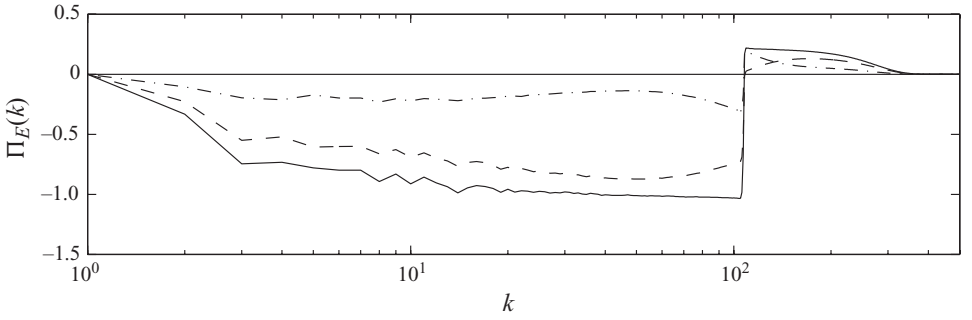

FIGURE 7. Energy flux, normalized by the mean flux in the range $k \in [10, 100]$, decomposed into total (solid), kinetic (dashed) and potential energy flux (dash-dotted) for $S1024E$. The zero line is indicated.

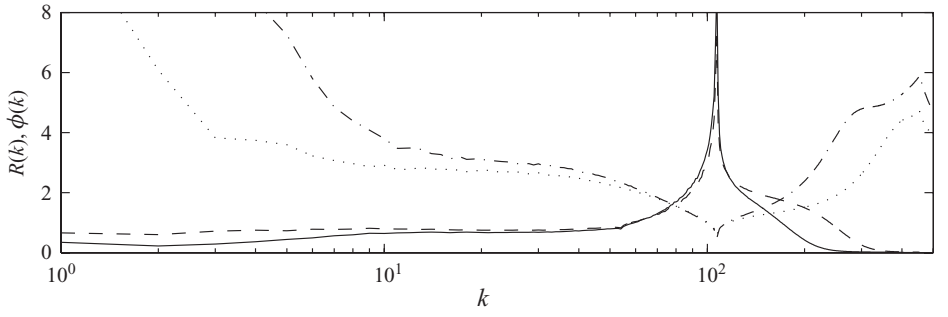

FIGURE 8. $R(k)$ for $S1024$ (solid), $S1024E$ (dashed) and $\phi(k)$ for $S1024$ (dash-dotted) and $S1024E$ (dotted).

energy tends to build up at large scales in absence of drag. Both simulations develop an inverse energy cascade range where

$$E(k) = \mathscr{K}\epsilon^{2/3}k^{-5/3}\,, \tag{3.4}$$

where the constant $\mathscr{K}$ has been estimated to $\sim$7.0 in $k \in [10, 100]$ for both simulations and ϵ is the energy flux. Charney's equipartition assumption is not fulfilled to the same degree as Charney isotropy, as the ratio $\phi(k)$ is a little bit larger than two (figure 8). This is reasonably due to the transfer of potential to kinetic energy. A distinct feature is the tendency for vorticity patches to organize into vertically elongated structures, that survive for long periods of time. They are not completely barotropic, but tend to wiggle a little bit with height, as seen in figure 9(b).

In all of the simulations presented so far, the growth of kinetic energy exceeds that of potential energy. This is a consequence of one of Charney's assumptions, namely that the horizontal scales of turbulence are small in comparison with the Rossby radius of deformation (see Pedlosky 1987), manifested in a transfer of potential to kinetic energy at large scales.

To test whether the inclusion of the β-effect violates the prediction of equipartition and Charney isotropy, we have run two simulations including the β-term. One is forced at large scales ($L1024EB$) and one is forced at small scales ($S1024EB$). Both include an Ekman drag. The physical picture of potential vorticity distribution in real space (figure 9c, d) differs significantly from what we have seen before, with pronounced zonally elongated structures, especially in $L1024EB$. This corresponds to an arrest of energy at a scale $k_\beta \sim \beta/\sqrt{\Omega}$, similar to the Rhines' scale (Rhines 1975),

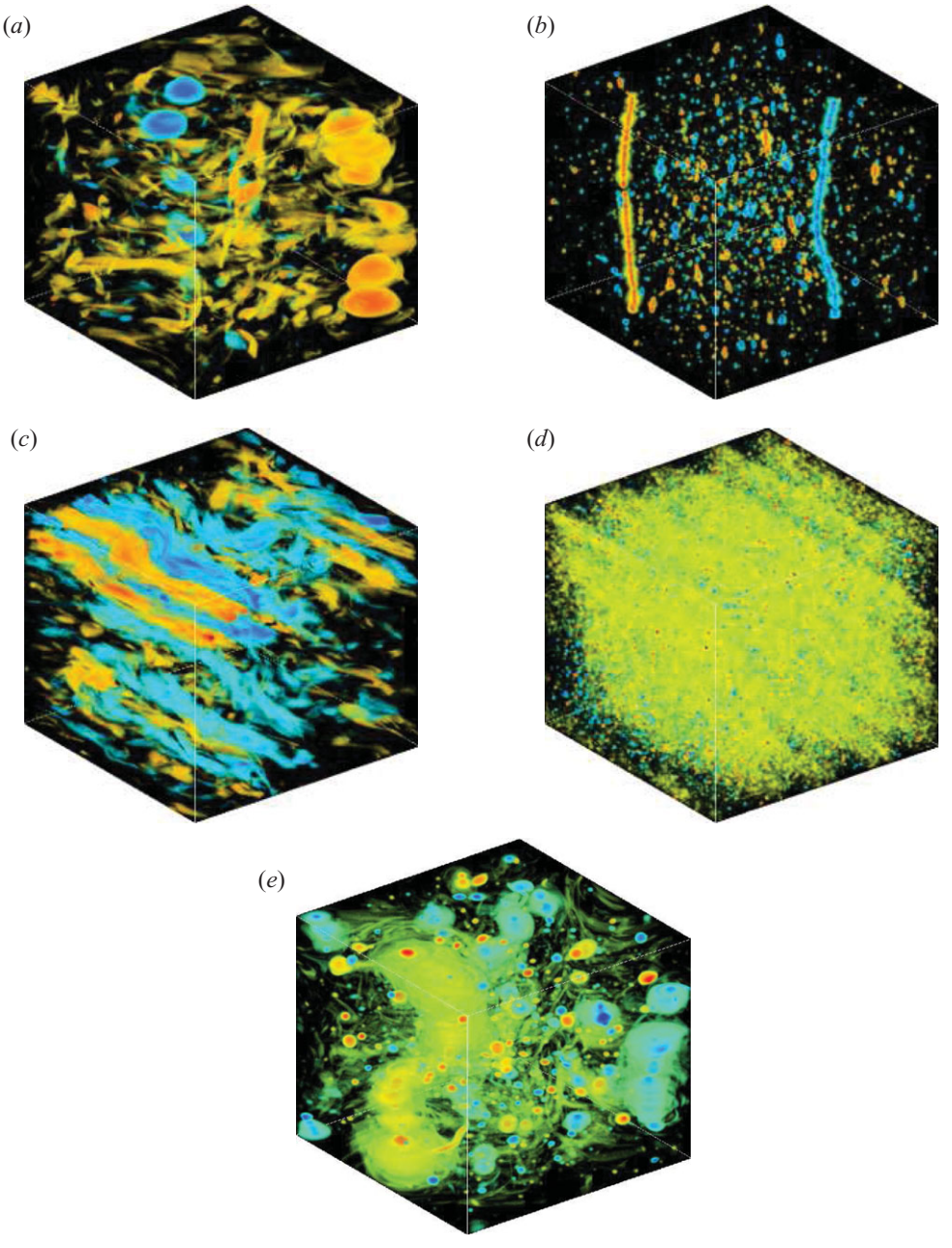

FIGURE 9. Snapshots of potential vorticity fields from $L1024E$ (a), $S1024E$ (b), $L1024EB$ (c), $S1024EB$ (d) and $L1024F$ (e). Blue colour correspond to negative values and red to positive.

where β has been set to 4.5 in both simulations. This scale is distinct in the meridional energy spectrum, but it is also clear from figure 9(c), that the width of the structures are similar in the vertical and the meridional direction. A glance at figure 11 reveals that there is approximate Charney isotropy over a broad range in wavenumber space in both simulations. In the large-scale driven simulation $L1024EB$, the ratio between the vertical energy spectrum and the 'meridional' energy spectrum is approximately

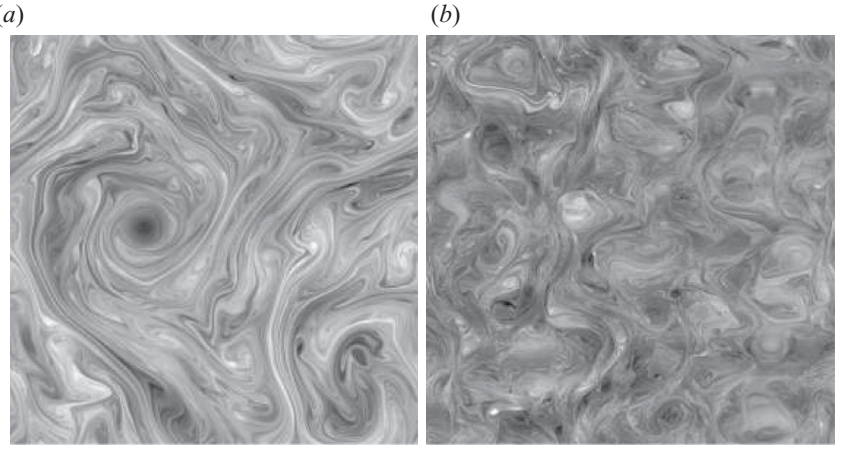

FIGURE 10. Snapshots of horizontal (a) and vertical (b) cross-sections of potential vorticity fields from $L1024E$. Dark colour corresponds to negative values and bright to positive.

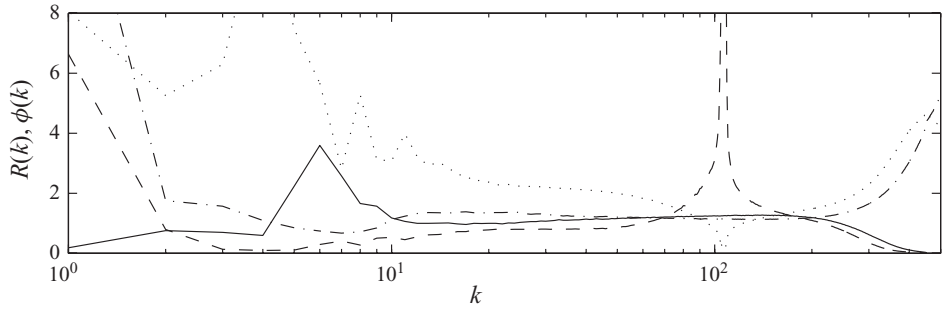

FIGURE 11. $R(k)$ for $L1024EB$ (solid) and $S1024EB$ (dashed), and $\phi(k)$ for $L1024EB$ (dash-dotted) and $S1024EB$ (dotted).

unity, indicating quantitative agreement of Charney isotropy. However, the ratio between the vertical and the 'zonal' spectrum is about three. Note that figure 11 represents the ratio based on a horizontal spectrum from the combined spectra of meridional and zonal components. In $S1024EB$, $R(k)$ is near unity for both of the horizontal components. In the latter simulation (figure 9d), the large-scale structures are more hidden due to the hazy appearance made up by the filamentation and the large number of small spherical vortices, induced by the forcing. There is approximate equipartition of potential and kinetic energy in the energy inertial range as $\phi(k)$ is near unity, except for the largest scales. Thus, the deviation from equipartition is not significant and Charney isotropy in the vertical and meridional direction is maintained while elongated structures (jets) form in the zonal direction, as a consequence of the planetary vorticity gradient.

We have also run two cases of freely decaying QG turbulence. One of the simulations ($L1024EF$) has been run from the end state of $L1024E$, whereas the other ($L1024F$) has been run from a randomly generated spectral initial state with unit potential enstrophy, partitioned into a spherical shell in the wavenumber range $k \in [11, 15]$, distributed with Gaussian amplitudes around $k_c = 13$. These two initial conditions were chosen to give room for a finite-time inverse energy cascade. We found that total energy is almost perfectly conserved, whereas kinetic and potential energy vary

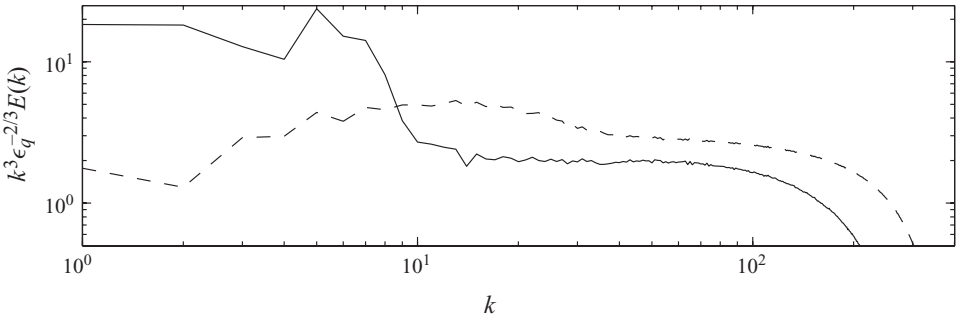

FIGURE 12. Compensated energy spectra, $k^3\epsilon_q^{-2/3}E(k)$, for $L1024EF$ (solid) and $L1024F$ (dashed).

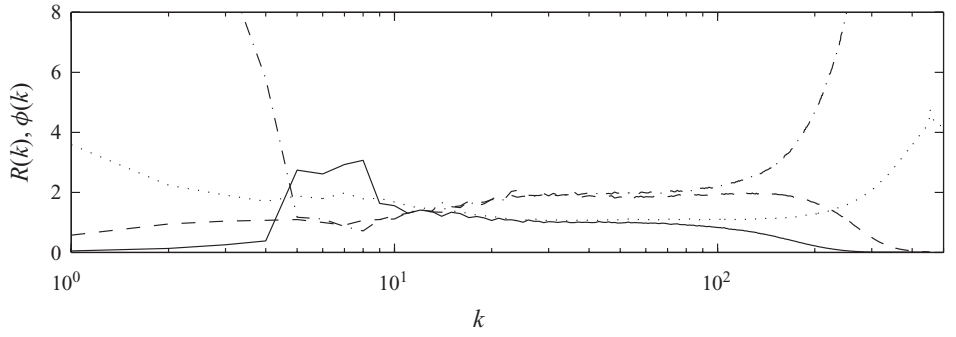

FIGURE 13. $R(k)$ for $L1024F$ (solid) and $L1024EF$ (dashed) and $\phi(k)$ for $L1024F$ (dash-dotted) and $L1024EF$ (dotted).

slightly in time as a consequence of internal interplay. The potential enstrophy decay is different between the simulations, with a decay rate $\sim t^{-1.35}$ in $L1024F$ and $\sim t^{-0.6}$ in $L1024EF$. It is reasonable to suspect that the presence of coherent structures in $L1024EF$ slows down the decay rate considerably. Despite the differences in the physical setting of the initial conditions, both simulations develop a $\sim k^{-3}$ direct enstrophy cascade regime over approximately one decade (see figure 12). In this range, $R(k) \sim 1$, as seen in figure 13, also showing Charney equipartition. Despite the tendency for the fluid to become more barotropic with time, there is a rich dynamics in the flow also after a long time period of several $O(100)$ non-dimensional time units (see figure 9*e*). Alignment tendencies are clear, but we also see a multitude of vortices of near spherical shape.

4. Conclusions

We have performed a number of simulations, ranging from small- to large-scale forcing, with and without Ekman drag and β-effect and two freely decaying simulations. They all support Charney's prediction of isotropic energy spectra and equipartition. It has also been confirmed that QG turbulence behaves much like two-dimensional turbulence in the sense that we obtain a clear forward potential enstrophy cascade and a dominating inverse energy cascade. The enstrophy cascade range is in agreement with the prediction of Kraichnan for two-dimensional turbulence. The inverse energy cascade scale as $\sim k^{-5/3}$, but is slightly steeper in the absence of a large-scale drag. Steeper spectra than $k^{-5/3}$ in the absence of large-scale drag or in

the presence of higher-order hypodiffusion have also been observed in simulations of two-dimensional turbulence (Danilov & Gurarie 2001). There is a weak forward energy cascade in the case when the forcing is placed at small scales, but it does not contribute to any significant departure from two-dimensional turbulent characteristics, not the least because it appears in a region where viscous effects are considerable and a forward enstrophy cascade governs the dynamics. In the case of freely decaying turbulence, Charney isotropy represents a preferred state, but there is also a tendency for coherent structures to develop. These affect the temporal statistics of decay rates.

Computer time was provided by SNIC (Swedish National Infrastructure for Computing) with a generous grant by the Knut and Alice Wallenberg Foundation.

REFERENCES

Alvelius, K. 1999 Random forcing of three-dimensional homogeneous turbulence. *Phys. Fluids* **11**, 1880.

Charney, J. G. 1971 Geostrophic turbulence. *J. Atmos. Sci.* **28**, 1087.

Danilov, S. & Gurarie, D. 2001 Forced two-dimensional turbulence in spectral and physical space. *Phys. Rev.* E **63**, 061208.

Dritschel, D. G., de la Torre Juarez, M. & Ambaum, H. P. 1999 The three-dimensional vortical nature of atmospheric and oceanic turbulent flows. *Phys. Fluids* **11**, 1512.

Gage, K. S. & Nastrom, G. D. 1986 Theoretical interpretation of atmospheric wavenumber spectra of wind and temperature observed by commercial aircraft during GASP. *J. Atmos. Sci.* **43**, 729.

von Hardenberg, J., McWilliams, J. C., Provenzale, A., Shchepetkin, A. & Weiss, J. B. 2000 Vortex merging in quasi-geostrophic flows. *J. Fluid Mech.* **412**, 331.

Herring, J. R. 1980 Statistical theory of quasi-geostrophic turbulence. *J. Atmos. Sci.* **37**, 969.

Hua, B. L. & Haidvogel, D. B. 1986 Numerical simulations of the vertical structure of quasi-geostrophic turbulence. *J. Atmos. Sci.* **43**, 2923.

Kraichnan, R. H. 1971 Inertial-range transfer in two- and three-dimensional turbulence. *J. Fluid Mech.* **47**, 525.

Lilly, D. K. 1989 Two-dimensional turbulence generated by energy sources at two scales. *J. Atmos. Sci.* **46**, 2026.

Lindborg, E. 1999 Can the atmospheric kinetic energy spectrum be explained by two-dimensional turbulence? *J. Fluid Mech.* **388**, 259.

McWilliams, J. 1989 Statistical properties of decaying geostrophic turbulence. *J. Fluid Mech.* **198**, 199.

McWilliams, J. 1990 The vortices of geostrophic turbulence. *J. Fluid Mech.* **219**, 387.

McWilliams, J., Weiss, J. B. & Yavneh, I. 1999 The vortices of homogeneous geostrophic turbulence. *J. Fluid Mech.* **401**, 1.

Nastrom, G. D. & Gage, K. S. 1985 A climatology of atmospheric wavenumber spectra of wind and temperature observed by commercial aircraft. *J. Atmos. Sci.* **42**, 950.

Pedlosky, J. 1987 *Geophysical Fluid Dynamics*, 2nd edn. Springer.

Reinaud, J. N., Dritschel, D. G. & Koudella, C. R. 2003 The shape of vortices in quasi-geostrophic turbulence. *J. Fluid Mech.* **474**, 175.

Rhines, P. B. 1975 Waves and turbulence on a beta-plane. *J. Fluid Mech.* **69**, 417.

Smith, L. M. & Waleffe, F. 1999 Transfer of energy to two-dimensional large scales in forced, rotating three-dimensional turbulence. *Phys. Fluids* **11**, 1608.

Tung, K. K. & Orlando, W. W. 2003 The k^{-3} and $k^{-5/3}$ energy spectrum of atmospheric turbulence: quasigeostrophic two-level model simulation. *J. Atmos. Sci.* **60**, 824.